Supporting Information

SI Material and Methods

Bacterial strains, Media and Culture conditions

Bacterial strains and plasmids used in this study are listed in Table S1. Luria-Bertani (LB) broth and LB broth minus salt were used as complex media and M9 with 0.05% casamino acid was used as minimal media. To maintain plasmids, antibiotics for selection used 100 μg/ml ampicillin, 25 μg/ml chloramphenicol or 50 μg/ml kanamycin. To select for chromosomal *hns* linker mutations and single copy integrants into att_{λ}, antibiotic concentrations were reduced to 20 μg/ml kanamycin and 7 μg/ml chloramphenicol.

Molecular Biology

DNA manipulations were carried out according to (1) using reagents from Qiagen and Fermentas. Polymerase chain reaction (PCR) used primers listed in Table S2 according to the manufacturer's instructions.

λ Red recombination

hns linker mutations and photoactivatable fluorescent protein fusion strains were constructed using λ-Red-mediated recombination (2). Briefly, linear DNA with flanking homologous sequences to target genomic DNA was electroporated into MG1655, a derivative of *E. coli* K-12 carrying pKD46, a plasmid that can express the Red system under tight control of a promoter. Successful recombination was selected by antibiotic-containing LB agar. Colonies were purified once and then further confirmed by PCR screening and DNA sequencing. To generate a chromosomal linker mutation of *hns* at its

original location, we first constructed a plasmid containing an *hns-kan* cassette. The *kan* cassette flanked by two FRT sites was PCR-amplified from pKD13 and inserted after the *hns* open reading frame (ORF). This plasmid was then used as the parental template to construct linker mutations using reverse-PCR following the Phusion site-directed mutagenesis protocol (Finnzymes). To construct chromosomal mutations, DNA fragments were PCR-amplified using primers matching the 5' *hns* sequence and *kan*-cassette with 54 base pairs of homology flanking sequence to the C-terminal DNA outside of the ORF. The liner DNA fragment was introduced into the wildtype strain MG1655 as described above. Photoactivatable fluorescent protein fusion strains were made using a similar approach. We first constructed a plasmid with a *PAmCherry*-Kan cassette after the last codon of *hns*. In between, a 12 amino acid flexible linker GSAGSAAGSGEF was used to connect the last codon of *hns* and the first codon of PAmCherry. This plasmid was used as template to construct the photoactivatable fluorescent protein linker deletion mutant (ΔL-PAmCherry).

Construction of a csgD promoter-gfp fusion

A c*sgD* promoter *gfp* chromosome fusion (PcsgD-*gfp*) was constructed in *E. coli* MG1655 using the CRIM system (3). A 755 bp *csgD* promoter DNA fragment was PCR-amplified and inserted in front of *gfp* to create the plasmid pCAH63-P*csgD-gfp*. This plasmid was purified and DNA sequencing confirmed the construct. It was then used to transform an *hns* wildtype and various linker substitutions carrying pINT-ts, a helper plasmid of the CRIM system, using electroporation. The recombinants were selected on LB agar plus chloramphenicol plates and confirmed by PCR screening as described (3).

Swarming motility assay

Cells were growth in LB medium at 37 °C overnight. 3 µl samples were spotted on a 0.3% soft agar plate containing 1% tryptone, 0.25% NaCl, and the plates were incubated at 37°C for 2-3 hours, and then transferred to RT overnight. The swarming zones were measured and then analyzed by averaging and normalizing to the wildtype strain.

GFP fluorescence measurements in single cells

Bacteria strains with PcsgD-*gfp* were cultured in LB minus salt and grown at 30°C, 100 rpm for 24h. 2 µl samples were removed from the culture and immobilized on slides with agarose pads (Thermoscientific, Brunswick Germany). Brightfield and fluorescence images were immediately obtained using a 100× objective on a DeltaVision Deconvolution Microscope (Olympus, Tokyo, Japan). GFP fluorescence was observed at excitation and emission wavelengths of 490 nm and 528 nm, respectively. At least 500 cells of each strain were collected from at least 5 distinct images for analysis. Segmentation and measurement of bacteria was performed using in-house Fiji macro. First, flat-field correction was applied by dividing each fluorescent image with a normalized background image. This background image was generated by averaging 10 background images acquired with the same settings. After correcting for uneven background, the image was background-subtracted using a rolling ball of 30-pixel radius. Segmentation of bacteria was performed using a Niblack thresholding method with a 20-pixel radius local region and an offset of -10. Manual splitting was performed on

clustered bacteria, if any. Using the segmented images, the fluorescence intensity for each cell was measured.

Overexpression and purification of proteins

The *E. coli* BL21 AI strain (Thermo Fisher Scientific) was used as a host for the overproduction of proteins His-tagged H-NS and H-NS mutants under pBAD promoter. The respective constructs are listed in Table S1. The detail overexpression and purification of H-NS and its mutants by His-tag affinity chromatography were described by (4). The fast protein liquid chromatography (FPLC) was used to analyze and purify H-NS and its mutants using a Superose12 10/300 GL column (GE) with an AKTA protein purification system (GE). The separation buffer used was 20mM Tris pH 7.6~8.0, 1M NaCl and 5mM β- mercaptoethanol.

AFM imaging

Glutaraldehyde-modified mica surfaces were used for all experiments and were prepared as follows. 0.1% solution of (3-aminopropyl)triethoxysilane (APTES) in deionized water was deposited on a freshly peeled mica for 15 min, followed by thorough rinsing with deionized water. 1% solution of glutaraldehyde in deionized water was then deposited on the APTES-modified mica for 15 min, followed by another rinsing with deionized water. The glutaraldehyde-modified mica was blown dry with N_2 gas prior to sample deposition. The sample was prepared as follows. A 755 bp *E. coli csgD* sequence was amplified and gel purified. 10 ng of this DNA was mixed with an appropriate concentration of H-NS or H-NS linker mutants and incubated for 15 min at room temperature in 50 mM KCl, 2 mM MgCl2, 10 mM Tris-HCl (pH 7.4) buffer. This mixture was then deposited on the glutaraldehyde-modified mica for 15 min, followed by

drying with N_2 gas. Images were acquired on a Bruker Dimension FastScan AFM system using the tapping mode with a silicon nitride cantilever (FastScan A, Bruker). Raw AFM images were processed using Gwyddion software. To obtain the relative height distribution histograms of H-NS-DNA complexes, a MATLAB code was used to apply a threshold and separate the DNA contour from the background. Pixel values of the DNA contour, which correspond to the relative height above the background, were then plotted as distribution histograms. A higher relative height indicates more H-NS bound to the DNA.

Construction of an active, chromosomally-encoded H-NS fluorescent fusion protein

Previous studies constructed a fluorescent protein fusion of H-NS in which mEos2 was fused to its C-terminus (5). Super-resolution imaging revealed an unusual localization pattern compared to other nucleoid-associated proteins such as HU. H-NS was visible as two discrete foci/bacterial cell, whereas HU was evenly distributed on the chromosome. A more recent comparison of different fluorophores reported that fluorescent protein fusions with a strong tendency to oligomerize (e.g., PAmCherry) could result in a number of imaging artifacts (6). Our recent attempts at constructing active fluorescent protein fusions identified a requirement for longer linkers between the protein of interest and the fluorescent protein (7, 8). Thus, we used a linker for constructing an H-NS fusion protein with photoactivatable mCherry (PAmCherry) and compared the activity of the fusion with wildtype H-NS. The H-NS-PAmCherry fusion was equivalent to the wildtype native protein, based on the motility assay (Fig. S6).

Sequential, multi-color single-molecule localization microscopy (SMLM)

Cells were grown in M9 medium up to OD_{600} ~0.2 at 37^{o}C with shaking. 10 μM of EdU was added and grown until OD_{600} ~0.6 (~1.5 cycles). Cells were then fixed with 1.5% PFA in PBS for 30 mins. They were then pelleted (6800 x g, 3 min), washed twice with PBS and lastly in 50 mM NH_4Cl_2 in PBS for 15 mins to reduce excess PFA. Cells were then treated with 0.1% Triton-X 100 in PBS for 30 mins followed by 2 PBS washes to prepare for click reaction of Alexa 647 to the DNA. They were then immobilized on glass chamber slides pre-cleaned with 3M KOH and pre-treated with 0.1 % poly-L-lysine. PALM imaging was first performed on H-NS-PAmCherry in PBS buffer. The PBS buffer was replaced by click-reaction buffer (100 mM Tris pH 8.0, 1 mM $CuSO_4$, 10 μM Alexa Fluor 647 azide, 100 mM ascorbic acid) and incubated for 30 mins to incorporate the Alexa 647 dye onto the nucleoid. The sample was then washed 2 times with PBS and once for 30 min with PBS. *d*STORM imaging of DNA-EdU-Alexa Fluor647 was performed in 50 mM Tris pH 8.0 buffer with 100 mM MEA (cysteamine hydrochloride).

Sequential, multiple color SMLM (PALM followed by *d*STORM) was performed as described previously (8, 9). Briefly, imaging was performed on a Nikon N-STORM Super-Resolution microscope. *Highly inclined and laminated optical sheet (HILO)* illumination was performed using a 561 or 647 nm laser line for PAmCherry and Alexa Fluor647, respectively. A 404 nm line was used for PAmCherry as an activating laser. About 20,000 frames were acquired using Micro-Manager (10) at an exposure time of 80 ms per frame for PAmCherry. 20,000 to 40,000 frames were acquired at 20 ms per frame for Alexa Fluor647. Data were analyzed with rapidSTORM (11). The localization precision determined by using the nearest neighbor based analysis (12) was 11.8 ± 0.2 nm for DNA-EdU-Alexa647 and 15.0 ± 0.2 nm for PAmCherry. Localizations in subsequent

frames within a radius of 20 nm were considered to be the same molecule and hence treated as a single localization. A Gaussian blur of the mean localization precision was applied to the reconstructed images using Fiji (13).

H-NS cluster analysis

The density-based spatial clustering of applications with noise (DBSCAN) algorithm detects clusters based on the local density of points within a search radius (14). DBSCAN requires two parameters, namely the minimum number of points required to form a cluster (P_{min}) and the search radius from a particular point (ε). As the density of localization obtained from PALM can influenced the two parameters, we vary P_{min} and ε until DBSCAN is able to properly recognize the clusters. Using the DBSCAN incorporated in the software LocAlization Microscopy Analyzer (LAMA) (15), we found that the value of $P_{min} = 40$ and $\varepsilon = 72$ nm best detected the clusters. The clusters detected are represented by circles with diameter representing the clusters size (Fig. S7). On average the cluster size was 273 ± 108 nm. Since the total number of H-NS localizations from PALM, and the number of H-NS localizations in the clusters were known, we can determine that 26.4% of H-NS molecules were in these clusters.

Quantitation of nucleoid size

Cells were grown to OD_{600} ~0.5 at 37^{o}C with shaking. Novobiocin (Sigma-Aldrich) was added (100 μg/ml) 30 mins before the cells were harvested (6800 x g for 3 mins). The cells were fixed with 1.5% PFA for 30 mins. Cells were pelleted and washed twice with PBS. *Permeabilization* was done using 0.1% Trixton X100 for 30 mins, followed by pelleting and washing twice with PBS. DAPI (10 μg/ml) was added to the cells. After 15 mins, the cells were pelleted and washed twice with PBS. Imaging was

performed using structured-illumination microscopy (SIM) on a W1 spinning Disk microscope (CSU-W1 Nikon, Japan) combined with the Live-SR system (Roper scientific) and equipped with a Plan-Apo λ 100x oil objective (1.45 NA, Nikon, Japan). DAPI was imaged with a 405 nm laser, emission 445/45 nm. Wild-field and DAPI images were acquired with a sCMOS camera (Prime 95B, Photometrics, USA). The raw images were processed to super-resolution images by using the Live-SR algorithm previously reported (16). The reconstructed pixel size is 65.87 nm x 65.87 nm. The brightfield image of the cells and the DAPI stained nucleoid were segmented using Fiji. The bright field segmentation was first processed by using enhance contrast (equalize histogram), Gaussian blur (1 pixel) and find edge. This allows the halos around the cells to be outlined. Auto local thresholding was then performed using the Otsu method (15 pixels), followed by binary-close. The segmented outline was then manually altered by filling the "hole" inside each cell outline. Analyze particles was used to obtain the ROI of each cell. As for the DAPI channel, Gaussian blur (1 pixel) and auto local thresholding using Otsu (5 pixels) was performed. The ROI from the cell outline was applied to the DAPI segmented image. Using the cell outline ROI, the length, width, area (corresponding to the cell outline) and integrated pixel intensity (corresponding to the nucleoid) were measured. The area of the nucleoid per cell was obtained by using the integrated pixel intensity divided by 255 (obtaining the number of pixels) and multiplied by the SIM-reconstructed pixel size (65.87 nm x 65.87 nm).

SptPALM

Cells were grown in M9 medium to OD_{600} ~0.6, centrifuged (6000xg, 3 min) and re-suspended in M9. 0.8 µl of the cells were then placed onto 1.5% low melting point

agarose pads (ThermoFisher) made with M9 on a glass slide with a small indentation (Toshinriko Co. Ltd, Japan). The cells were then sandwiched with a cover glass (Deckglaeser) pre-cleaned with 3M KOH. SPT experiments were performed using similar settings as SMLM, except that 50,000 frames were acquired at an exposure time of 15 ms, resulting in ~17 ms per frame (calculated by dividing total frames by total time acquired). Spots were detected and connected using the Fiji tracking plugin TrackMate. Tracks were then further analyzed using custom codes written in MATLAB. Only tracks with more than 5 spots were used for data analysis. Given that the diameter of *E. coli* in our experiment is only ~1 μm, a large portion of the total molecules are in focus and tracked. Since only the x – y movement in the focal plane is recorded, the 3D trajectories are essentially considered as 2D diffusions, i.e., x – y displacement described with a 2D model is used to extract the value of *D,* which is independent of dimension. Using the mean square displacement (MSD) $<r^2>$ for 2D diffusion, the diffusion coefficient *D* can be determined:

$$< r^2 > = 4D\tau \quad (1)$$

where τ is the time lag (acquisition time per frame). *D* from each individual track was calculated from the slope of $<r^2>$ generated from the first three time lags (where the MSD is most linear), and plotted on a histogram.

Since each track has a *D* calculated from the MSD, the tracks could be color-coded to show the value of *D* in the cell. However, the tracks overlaid on each other prevent one from being able to obtain much information about the distribution of *D* in the cell. Therefore, the tracks were converted into a diffusion map. The x-y vector coordinates of the spots from each track (with a certain *D* value) were converted into pixel coordinates

(50 nm pixel size bin) and the pixels given the value of D. The D values for pixels with more than one spot from either the same or different tracks were averaged.

The cumulative probability distribution (CPD) method was used to differentiate between molecules with different diffusion coefficients D (17). A three-component diffusion model best fitted our data. For diffusing molecules with three different D values, the probability that a particle starting at the origin will be found within a circle of radius r at time τ is given by:

$$P(r^2,\tau) = 1 - \left[F_1 \exp\left(-\frac{r^2}{<r^2>_1}\right) + F_2 \exp\left(-\frac{r^2}{<r^2>_2}\right) + (1 - F_1 - F_2) \exp\left(-\frac{r^2}{<r^2>_3}\right)\right] \quad (2)$$

where F_1 and F_2 are the fractions of molecules with mean squared displacements $<r^2>_1$ and $<r^2>_2$ respectively. Using Eq (1), this can be written as

$$P(r^2,\tau) = 1 - \left[F_1 \exp\left(-\frac{r^2}{4D_1\tau}\right) + F_2 \exp\left(-\frac{r^2}{4D_2\tau}\right) + (1 - F_1 - F_2) \exp\left(-\frac{r^2}{4D_3\tau}\right)\right] \quad (3)$$

The individual diffusion coefficients D_i can then be obtained from a fit of a CPD plot of probability against $r^2/4\tau$ (18).

We term the diffusion coefficient obtained here an 'apparent diffusion coefficient', D^* as its value is influenced by the small movement from the immobilized live bacteria, movement of the nucleoid, and localization error of a moving molecule during acquisition. In addition, confined diffusion within the small bacterial volume leads to an under-estimate of D (19).

The D_3 value of the unbound form of wildtype H-NS is different from that of the ΔL mutant. In addition the D_3 value are relatively small compared to a free diffusing fluorescent protein (D^* of ~7.3 μm²/s (20)). The reason can be explained by the FPLC profile of wildtype H-NS and ΔL (Fig. S4). Both proteins exist as oligomers when not bound to DNA, resulting in a lower than expected D_3. The difference in the value of D_3

between the wildtype and ΔL is most likely due to the level of oligomerization. In Fig. S4, ΔL has an elution profile with a lower molecular size shoulder compared to the wildtype.

Molecular dynamics simulations

All-atom molecular dynamics simulation was based on the crystal structure of an H-NS segment that includes the linker and C-terminus (amino acids 91-137; PDB 1HNR (21)) and B-DNA (sequence: ATTTTAATATAACGAGTTAC) built by x3DNA software (22). DNA and protein structures were solved in explicit water TIP3P containing 50 mM KCl. The DNA and protein structures were placed ~2.5 nm apart with a minimum distance of 1 nm to the box walls before simulation commenced. Nine independent simulation trajectories based on different initial conformations were performed for up to 500 ns. All molecular dynamics simulations were performed using Gromacs 5.1.1 (23) with the ff99sb-ildn-NMR force field (24).

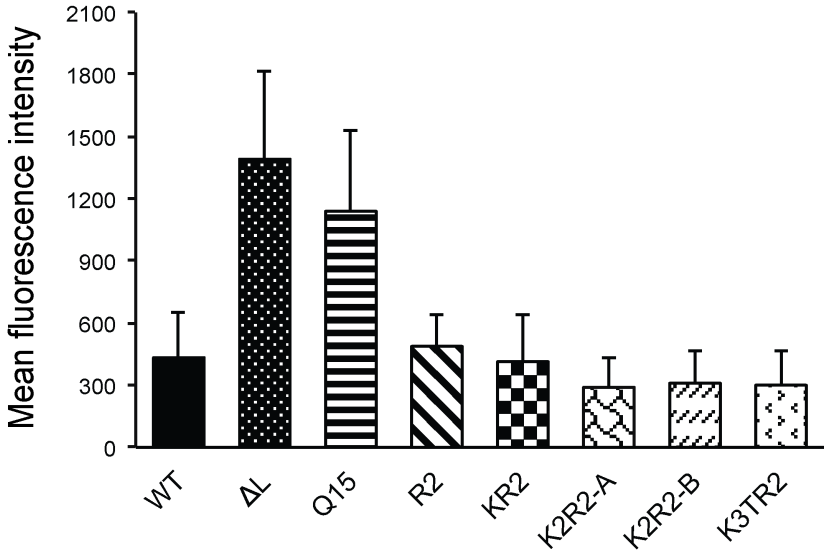

Fig. S1. H-NS linker mutants affect transcriptional activation of the *csgD* promoter.
GFP fluorescence of a P*csgD-gfp* transcriptional fusion was determined by fluorescence microscopy (see methods). The mean fluorescence of > 500 single cells from at least five separate images was plotted. Wildtype H-NS repressed *csgD* transcription (25), the ΔL and Q15 mutants were unable to repress *csgD*. Addition of positive-charged residues into the Q15 linker partially restored *csgD* repression. Mutants with at least two lysines and two arginines (K2R2-A, K2R2-B and K3TR2) exhibited maximum repression of *csgD*.

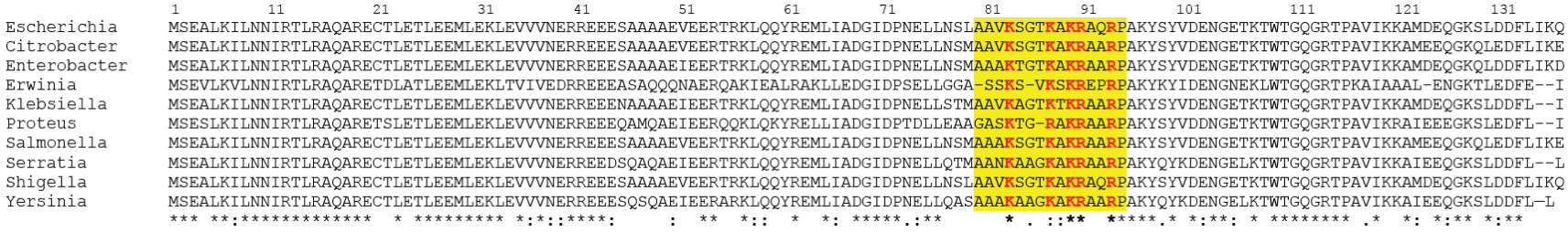

Fig. S2. Alignment of multiple *hns* sequences.

Alignment of H-NS protein using ClustlW. The linker is highlighted in yellow. An * (asterisk) indicates positions which have a single, fully conserved residue. A : (colon) indicates conservation between groups of strongly similar properties - scoring > 0.5 in the Gonnet PAM 250 matrix. A . (period) indicates conservation between groups of weakly similar properties - scoring =< 0.5 in the Gonnet PAM 250 matrix.

.

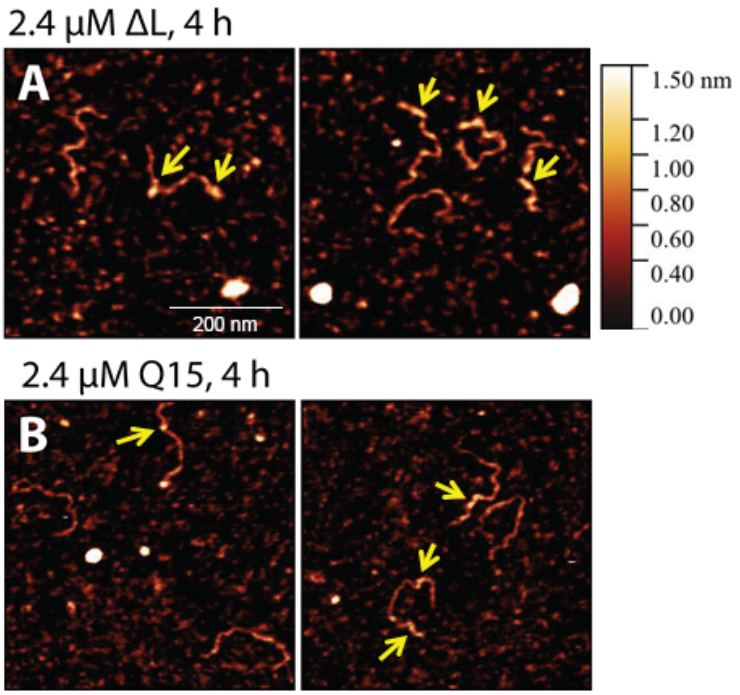

Fig. S3. The inability of ΔL and Q15 mutants to form a stiffened filament is not due to reduced binding affinity.

At higher concentrations and longer incubation times, ΔL *(A)* and Q15 *(B)* mutants form segregated small patches of filaments on P*csgD* DNA. H-NS mutant protein concentration was 2.4 μM, 4h incubation.

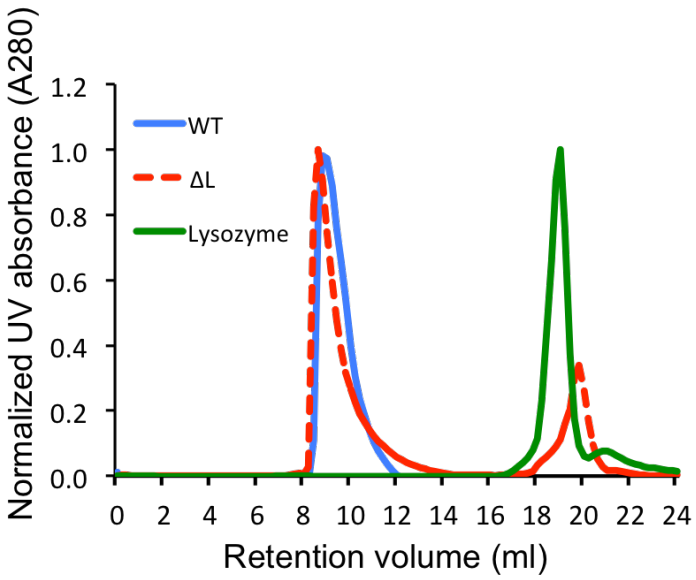

Fig. S4. Size exclusion chromatograms of wildtype (blue solid line) and ΔL (red dashed line) H-NS proteins.

Wildtype or ΔL H-NS was purified using Talon affinity *resin* and then separated on a Superose12 10/300 GL column using FPLC. The molecular weights of the monomer, His-tagged wildtype and ΔL H-NS were 15-16 kDa. Lysozyme, a similar size protein (14.3kDa), was chosen as an internal size standard (green). Lysozyme elutes at 18.97 ml, whereas the major peaks of wildtype H-NS and ΔL elute at ~8.8 ml. This indicates that both wildtype and ΔL H-NS form oligomers in solution. The peak at 19.8 ml was most likely due to a small protein contaminant eluted from the Talon resin.

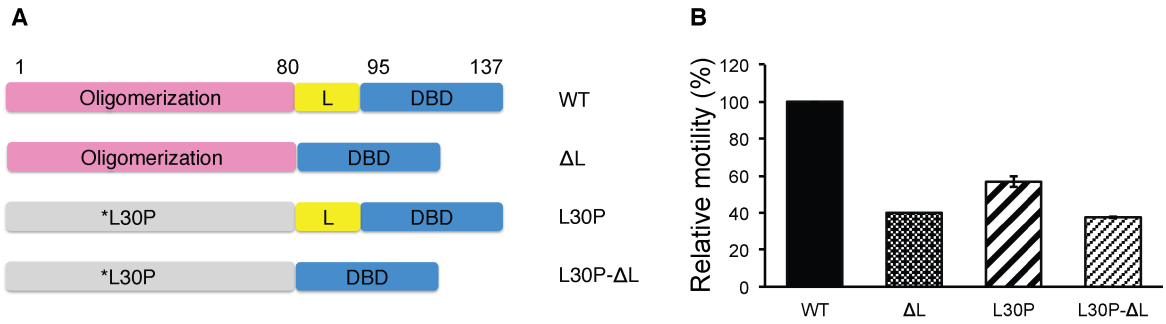

Fig. S5. The dimerization mutant L30P does not have an additional effect on DNA binding of the ΔL linker mutant.

(A) Illustrates the protein architecture of the mutants. *(B)* Compares the motility of linker deletion mutant ΔL, dimerization mutant L30P and the double mutant. The swarm diameter was measured and normalized to wildtype strain MG1655. The swarm diameter of ΔL was 40% of wildtype, whereas L30P was 57% of wildtype. The swarm of the double mutant (L30P-ΔL) was 38% of wildtype, essentially identical to ΔL.

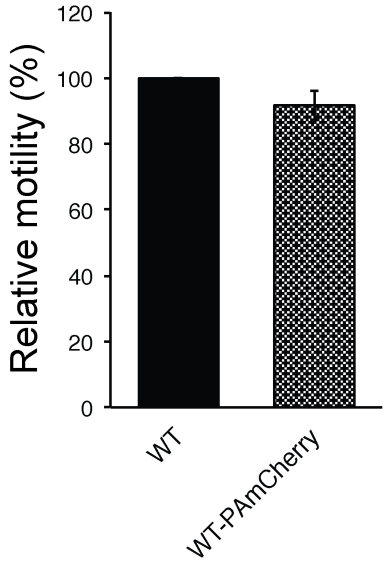

Fig. S6. An H-NS-PAmCherry fusion retained full activity as determined by swarming motility assay.

The diameter of the swarm of H-NS-PAmCherry was measured (92% ± 4%) and compared to wildtype H-NS lacking a fusion (100%).

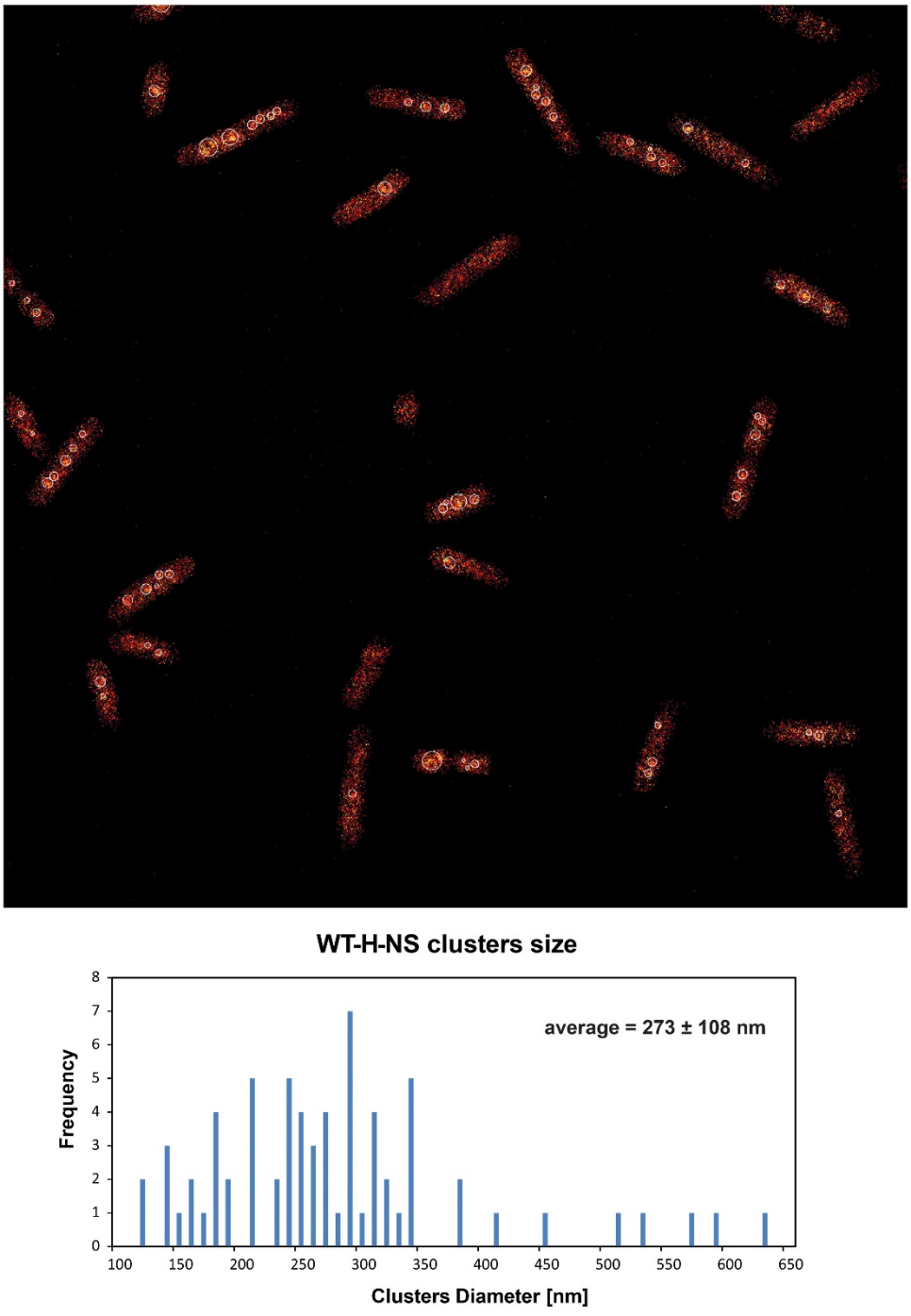

Fig. S7. Wildtype H-NS cluster analysis.

The white circles indicate the cluster size detected by DBSCAN (P_{min} = 40 and ε = 72 nm) on a PALM image of wildtype H-NS. The diameter of the clusters were plotted in a histogram. The average cluster size was 273 ± 108 nm.

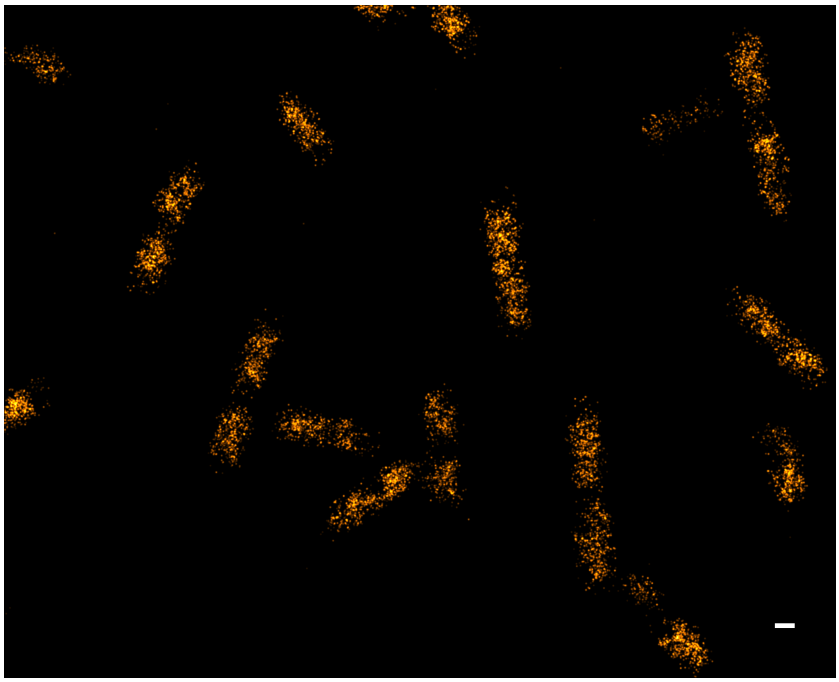

Fig. S8. A representative, reconstructed PALM image of H-NS-PAmCherry.
H-NS does not form foci when grown in LB (rich media). The localization pattern was similar to the *E. coli* nucleoid structure observed during rapid growth (26) and was not a consequence of the fusion protein.

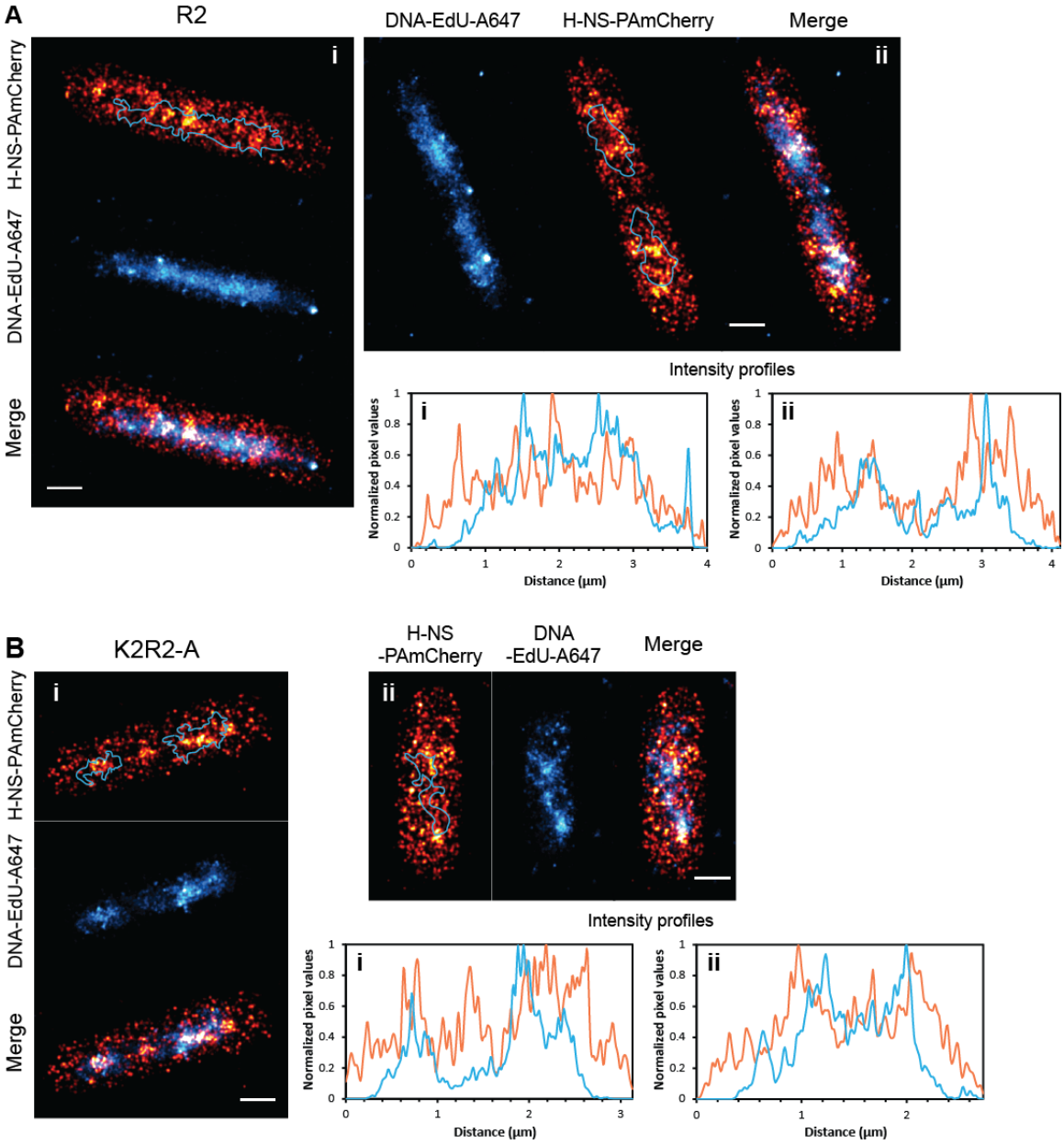

Fig. S9. Two-color SMLM of the R2 and R2K2-A mutants. *(A)* R2 H-NS mutant. *(B)* R2K2-A H-NS mutant. Cyan lines outline the nucleoid. Intensity profiles indicate the DNA-EdU-Alexa 647 signal (cyan plot) and the H-NS-PAmCherry signal (orange plot). Scale bar is 0.5 μm.

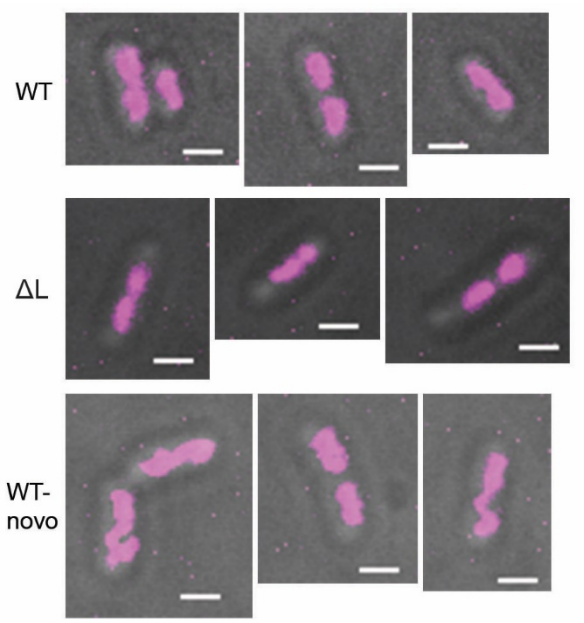

Fig. S10. Representative SIM images of bacterial cells stained with DAPI.
The nucleoid size of wildtype cells was 0.43 ± 0.11 μm^2 (n = 107). The nucleoid size of the ΔL mutant cells was smaller, at 0.38 ± 0.10 μm^2 (n = 112). Wildtype cells treated with 100 μg/ml novobiocin for 30 mins showed a more relaxed nucleoid (0.51 ± 0.15 μm^2, n = 150).

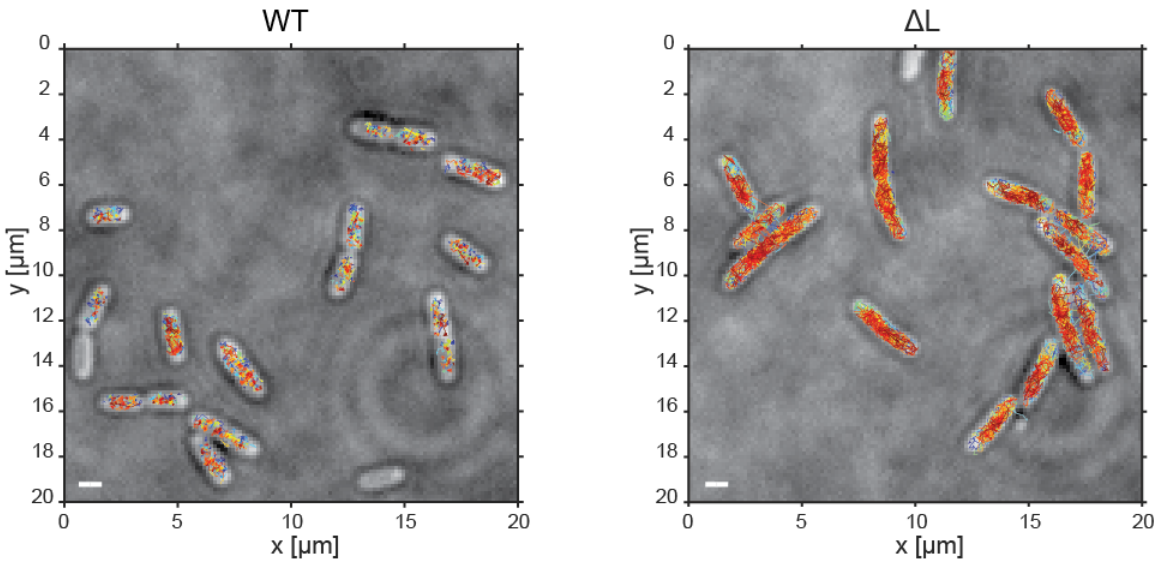

Fig. S11. Representative sptPALM of wildtype and ΔL H-NS.
The tracks in WT were less mobile compared to ΔL.

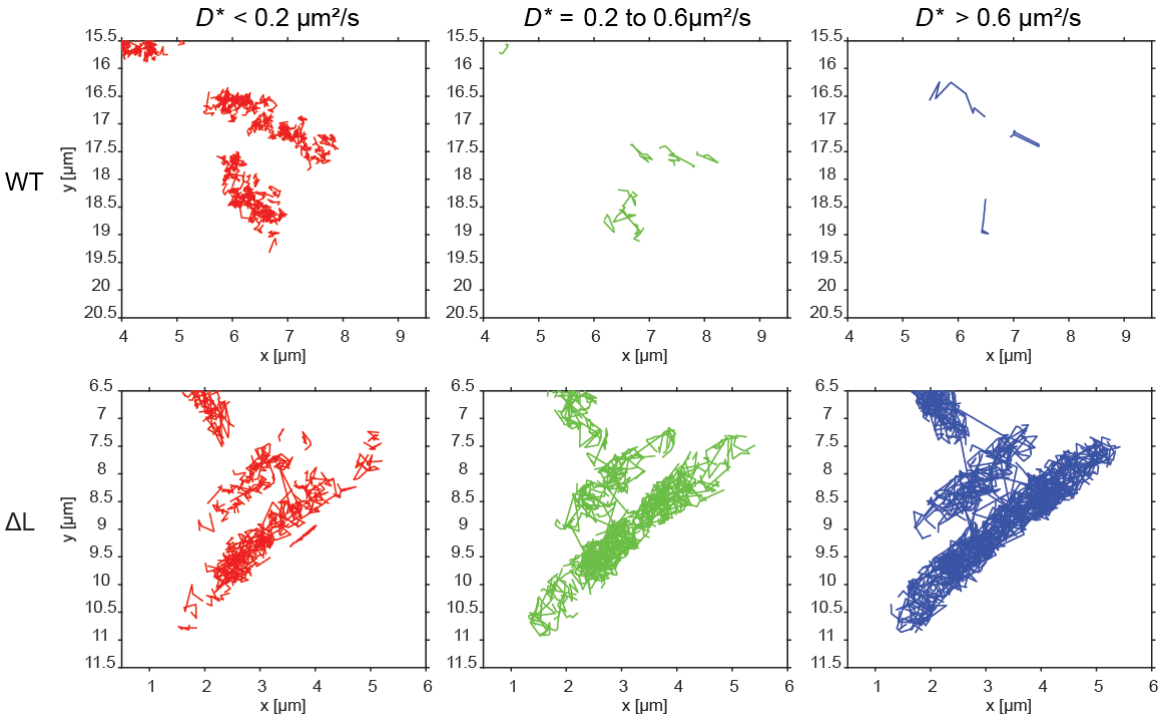

Fig. S12. Representative sptPALM tracks sorted into different *D ranges.**

Apparent diffusion coefficient *D** for each induvial track was calculated from the MSD. The distribution of tracks towards higher values of *D** can be observed for ΔL compared to WT.

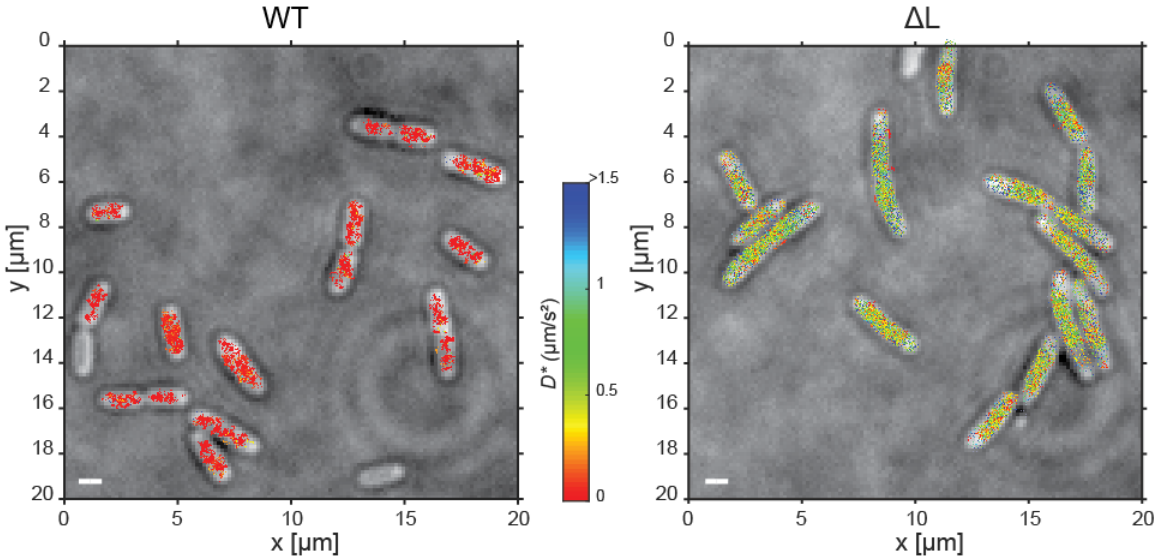

Fig. S13. Representative diffusion maps of wildtype and ΔL H-NS.

Spots in all tracks were converted into pixel coordinates. Pixel sizes were 50 nm. The color bar indicates the distribution of apparent diffusion coefficients *D**. In the wildtype, *D** were small and localized in clusters in the center of the cell. On the other hand, in ΔL, *D** were larger and the tracks were distributed throughout the cell with a slightly denser region in the center of the cell.

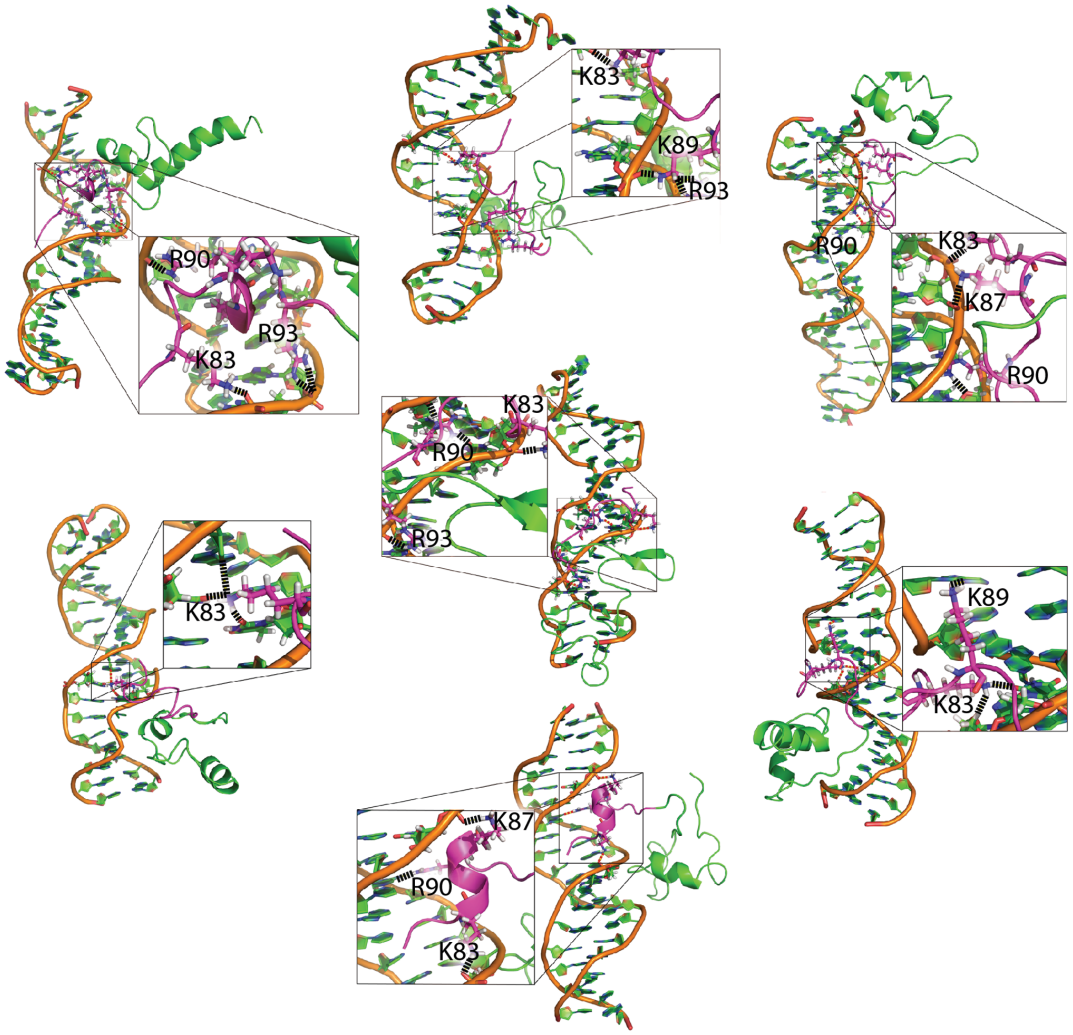

Fig. S14. Snapshots from nine, independent trajectories of molecular dynamics simulations with different initial conformations.

The C-terminus of H-NS (amino acids 95-137) is indicated in green and the linker (amino acids 80-94) is indicated in magenta. All trajectories feature a stable attraction between DNA and the linker of H-NS. Key residues forming hydrogen bonds were shown in stock representation and hydrogen bonds were shown in black dashed lines.

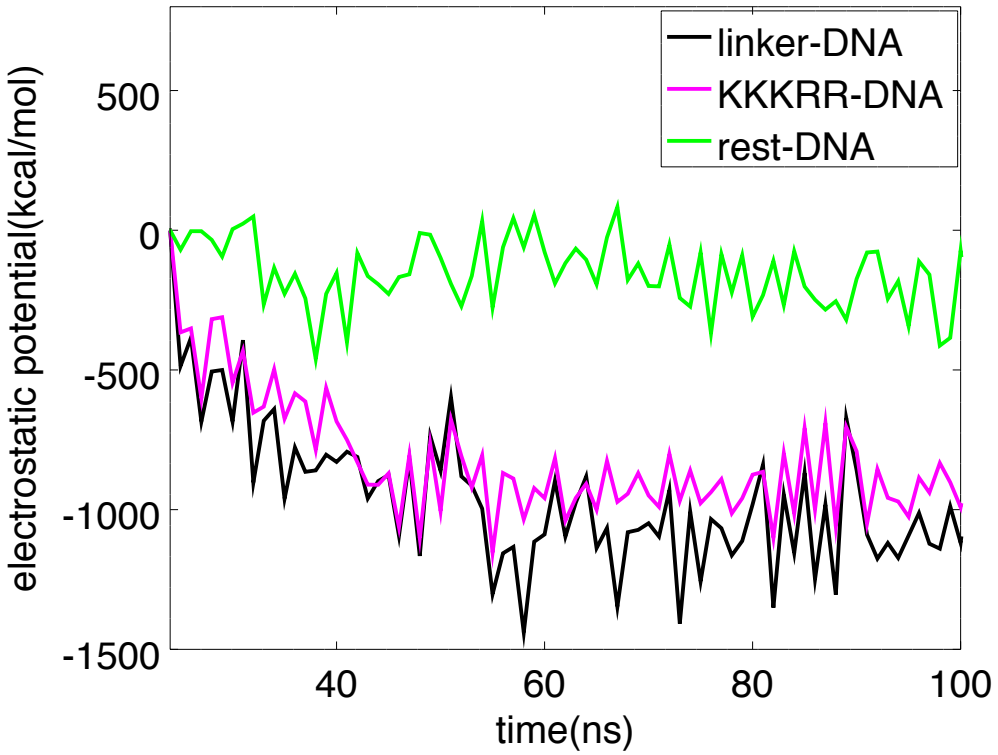

Fig. S15. The electrostatic potential between different regions of H-NS with DNA. All residues in the linker with DNA are shown in black. In magenta, only residues K83, K87, K89 and R90, R93 with DNA were considered. In green, the remaining residues in the linker with DNA were considered. The potential decrease was mainly contributed from K83, K87, K89 and R90, R93.

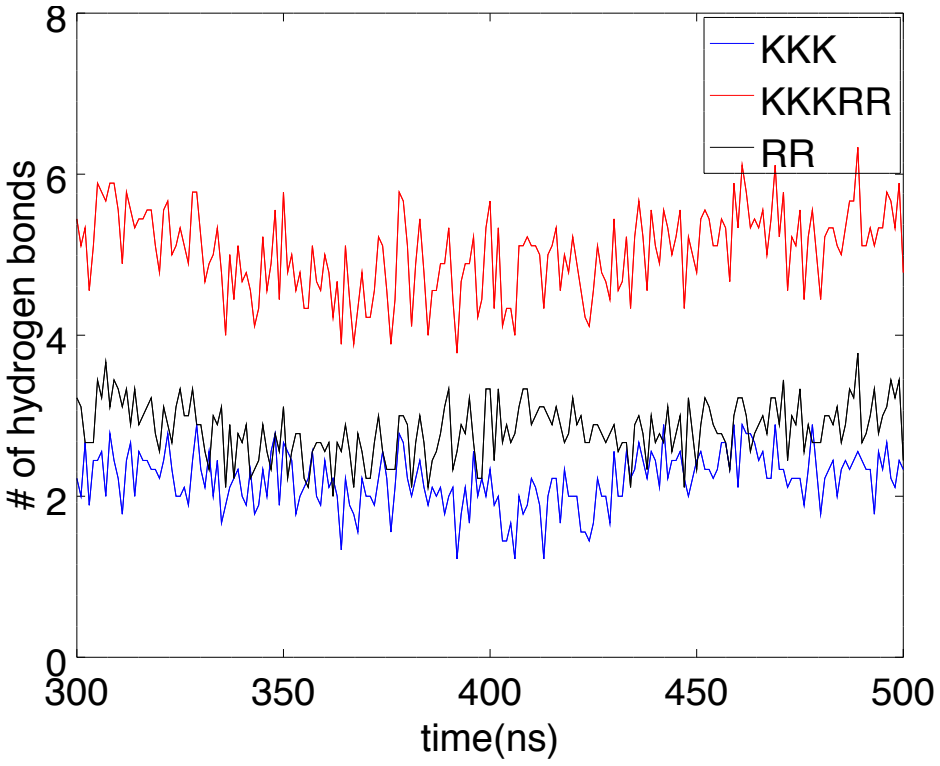

Fig. S16. The number of hydrogen bonds formed between different charged amino acid residues with DNA.

The last 200 ns of molecular dynamics simulation was shown.

Table S1. Strains and plasmid vectors used in this study

Strain/plasmid	Description	Reference/Source
Bacteria		
Wildtype	*E coli K12* derivative, MG1655	ATCC® 700926
Δ*hns*	MG1655 *hns*::*tetRA*	Lab strain collection
ΔL	MG1655 *hns* linker deletion	This study
Q15	MG1655 *hns* liker replaced by QQQQQQQQQQQQQQQ	This study
R2	MG1655 *hns* liker replaced by QQQQQQQQQQRQQRQ	This study
KR2	MG1655 *hns* liker replaced by QQQQQQQKQQRQQRQ	This study
K2R2-A	MG1655 *hns* liker replaced by QQQKQQQKQQRQQRQ	This study
K2R2-B	MG1655 *hns* liker replaced by QQQQQQQKQKRQQRQ	This study
K3TR2	MG1655 *hns* liker replaced by QQQKQQTKQKRQQRQ	This study
K2R2-short	MG1655 *hns* liker replaced by QKQKRQQRQ	This study
K2R2-N	MG1655 *hns* liker replaced by QQQQQQQQQQQQQKQKRQQRQ	This study
K2R2-C	MG1655 *hns* liker replaced by QKQKRQQRQQQQQQQ	This study
K4R4	MG1655 *hns* liker replaced by QKQKRRQKQKRQQRQ	This study
L-A5	MG1655 *hns* liker replaced by AAVASGTAAAAAQAP	This study
WT-PcsgD-*gfp*	PcsgD-*gfp* on MG1655	This study
ΔL-PcsgD-*gfp*	PcsgD-*gfp* on ΔL	This study
Q15-PcsgD-*gfp*	PcsgD-*gfp* on Q15	This study
R2-PcsgD-*gfp*	PcsgD-*gfp* on R2	This study
KR2-PcsgD-*gfp*	PcsgD-*gfp* on KR2	This study
K2R2-A-PcsgD-*gfp*	PcsgD-*gfp* on K2R2-A	This study
K2R2-B-PcsgD-*gfp*	PcsgD-*gfp* on K2R2-B	This study
K3TR2-PcsgD-*gfp*	PcsgD-*gfp* on K3TR2	This study
WT-*PAmCherry*	MG1655 *hns::PAmCherry*	This study
ΔL-*PAmCherry*	MG1655 *hns* ΔL*::PAmCherry*	This study
R2-*PAmCherry*	R2 *hns::PAmCherry*	This study
K2R2-A-*PAmCherry*	K2R2-A *hns::PAmCherry*	This study
Plasmids vectors		
pKD46	λ-Red recombinase expression plasmid, Amp^R	(2)
pINT-ts	CRIM helper plasmid	(3)
pCAH63	CRIM cloning vector for PcsgD-*gfp* insertion	(3)
pBAD	Cloning vector containing araBAD promoter for hns and hns-PAmcherry cloning	Invitrogen

Table S2. Primers used in this study

Primer Name	Sequences (5' to 3')
hns-5'-F2	AGCGAAGCACTTAAAATTCTGAAC
hns3UTR-P1	CAATAAAAAATCCCGCCGCTGGCGGGATTTTAAGCAAGTGCAATCTACAAAAGAG TGTAGGCTGGAGCTGCTTC
hns-P4-F	ATTTCCTGATCAAGCAATAAATTCCGGGGATCCGTCGACC
pBAD-reverse-P1	GTTCTGATTTAATCTGTATCGTGTAGGCTGGAGCTGCTTC
hns-C-terminal-R	TTATTGCTTGATCAGGAAATCGT
pBAD-R-overlap-F	GATACAGATTAAATCAGAACGCAG
hns-linker1-R2	GAATTCGCCAGAACCAGCAGC
kan-P4	ATTCCGGGGATCCGTCGACC
Linker1-PAmcherry	GCTGGTTCTGGCGAATTCATGGTGAGCAAGGGCGAGGA
P4-PAmcherry-R	TCGACGGATCCCCGGAATCTACTTGTACAGCTCGTCCATG
hns-ΔL-F	GCAAAATATAGCTACGTTGACGAAA
hns-ΔL-R	AAGGCTATTCAGCAGCTCGTTC
Q15-hns-F	AGCAGCAGCAACAGCAGCAGGCAAAATATAGCTACGTTGACGAAA
Q15-hns-R	GTTGCTGTTGCTGCTGCTGTTGCTGAAGGCTATTCAGCAGCTCGTT
R2-F	CAGCAACAGCAGCAGCAACAGCAACAGCAGCGTCAACAGCGTCAGGCAAAATATAGCT ACGTTGACGAAA
KR2-F	CAGCAACAGCAGCAGCAACAGAAACAGCAGCGTCAACAGCGTCAGGCAAAATATAGCT ACGTTGACGAAA
K2R2-A-F	CAGCAACAGAAACAGCAACAGAAACAGCAGCGTCAACAGCGTCAGGCAAAATATAGCT ACGTTGACGAAA
K2R2-B-F	CAGCAACAGCAGCAGCAACAGAAACAGAAACGTCAACAGCGTCAGGCAAAATATAGCT ACGTTGACGAAA
K3TR2-F	CAGCAACAGAAACAGCAAACCAAACAGAAACGTCAACAGCGTCAGGCAAAATATAGCT ACGTTGACGAAA
K2R2-Short-F	CAGAAACAGAAACGTCAACAGCGTCAG
K2R2-N-F	AAACAGAAACGTCAACAGCGTCAGGCAAAATATAGCTACGTTGACGAAA
K2R2-N-R	CTGCTGCTGTTGCTGTTGCTGCTGCTGTTGCTG
K2R2-C-F	CAGAAACAGAAACGTCAACAGCGTCAGCAGCAGCAACAGCAGCAGGCAAAATAT
K4R4-R	CCTCCGCTTCTGCTTCTGAAGGCTATTCAGCAGCTCGTTC
L-A5-F	GCAGCTGCAGCTGCTCAGGCTCCGGCAAAATATAGCTACGTTGACGAAA
L-A5-R	GGTGCCAGATGCAACGGCGGCAAGGCTATTCAGCAG
pCAH63-PcsgD-F	TAGTGTCTTCAAGAATTCTGTTGTCACCCTGGACCTGGTC
pCAH63-PcsgD-R	TTCTTCTCCTTTACTCATGATGAAACCCCGCTTTTTTTATTGATC
pCAH63-EcoRI	CCAAGAATTCTTGAAGACACTAGTTCCGGACA
GFP-F	ATGAGTAAAGGAGAAGAACTTTTC
PcsgD-F	TGTTGTCACCCTGGACCTGGT
PcsgD-R	GATGAAACCCCGCTTTTTTTATTGATC

Table S3. Three diffusion component CPD fits of the tracks obtained from sptPALM of the different H-NS constructs

WT	D_1 = 0.04 ± 0.01 35% Bound	D_2 = 0.12 ± 0.01 60%	D_3 = 1.05 ± 0.15 5% Unbound
K2R2-A	D_1 = 0.04 ± 0.01 53% Bound	D_2 = 0.12 ± 0.01 41%	D_3 = 1.14 ± 0.14 6% Unbound
R2	D_1 = 0.05 ± 0.01 34% Bound	D_2 = 0.19 ± 0.01 43%	D_3 = 0.98 ± 0.05 23% Unbound
ΔL	D_1 = 0.12 ± 0.01 21% Bound	D_2 = 0.54 ± 0.03 55% Intermediate	D_3 = 1.96 ± 0.11 24% Unbound

References

1. Sambrook J & Maniatis T (1989) *Molecular Cloning: A Laboratory Manual* (Cold Spring Harbor Laboratory Press, Cold spring Harbor, NY).
2. Datsenko KA & Wanner BL (2000) One-step inactivation of chromosomal genes in Escherichia coli K-12 using PCR products. *Proc Natl Acad Sci U S A* 97(12):6640-6645.
3. Haldimann A & Wanner BL (2001) Conditional-replication, integration, excision, and retrieval plasmid-host systems for gene structure-function studies of bacteria *J. Bacteriol.* 183:6384-6393.
4. Liu Y, Chen H, Kenney LJ, & Yan J (2010) A divalent switch drives H-NS/DNA-binding conformations between stiffening and bridging modes. *Genes Dev* 24(4):339-344.
5. Wang W, Li GW, Chen C, Xie XS, & Zhuang X (2011) Chromosome organization by a nucleoid-associated protein in live bacteria. *Science* 333(6048):1445-1449.
6. Wang S, Moffitt JR, Dempsey GT, Xie XS, & Zhuang X (2014) Characterization and development of photoactivatable fluorescent proteins for single-molecule-based superresolution imaging. *Proc Natl Acad Sci U S A* 111(23):8452-8457.
7. Foo YH, Gao Y, Zhang H, & Kenney LJ (2015) Cytoplasmic sensing by the inner membrane histidine kinase EnvZ. *Prog Biophys Mol Biol* 118(3):119-129.
8. Foo YH, Spahn C, Zhang H, Heilemann M, & Kenney LJ (2015) Single cell super-resolution imaging of E. coli OmpR during environmental stress. *Integr Biol (Camb)* 7(10):1297-1308.
9. Spahn C, Francesca Z-C, Ulrike E, & Heilemann M (2015) Correlative super-resolution imaging of RNA polymerase distribution and dynamics, bacterial membrane and chromosomal structure in Escherichia coli. . *Methods and Applications in Fluorescence* 3:0140005.
10. Edelstein A, Amodaj N, Hoover K, Vale R, & Stuurman N (2001) Computer Control of Microscopes Using μManager. *Current Protocols in Molecular Biology*, (John Wiley & Sons, Inc.).
11. Wolter S*, et al.* (2012) rapidSTORM: accurate, fast open-source software for localization microscopy. *Nat Methods* 9(11):1040-1041.

12. Endesfelder U, Malkusch S, Fricke F, & Heilemann M (2014) A simple method to estimate the average localization precision of a single-molecule localization microscopy experiment. *Histochem Cell Biol* 141(6):629-638.
13. Schindelin J*, et al.* (2012) Fiji: an open-source platform for biological-image analysis. *Nat Methods* 9(7):676-682.
14. Esther M, Kriegel H-P, Sander J, & Xu X (1996) A density-based algorithm for discovering clusters in large spatial databases with noise. *Proceedings of the Second International Conference on Knowledge Discovery and Data Mining* eds Simoudis E, Han J, & Fayyad UM (AAAI Press), pp 226-231.
15. Malkusch S & Heilemann M (2016) Extracting quantitative information from single-molecule super-resolution imaging data with LAMA - LocAlization Microscopy Analyzer. *Sci Rep* 6:34486.
16. York AG*, et al.* (2013) Instant super-resolution imaging in live cells and embryos via analog image processing. *Nat Methods* 10(11):1122-1126.
17. Schutz GJ, Schindler H, & Schmidt T (1997) Single-molecule microscopy on model membranes reveals anomalous diffusion. *Biophys J* 73(2):1073-1080.
18. Gebhardt JC*, et al.* (2013) Single-molecule imaging of transcription factor binding to DNA in live mammalian cells. *Nat Methods* 10(5):421-426.
19. Chen TY*, et al.* (2015) Quantifying Multistate Cytoplasmic Molecular Diffusion in Bacterial Cells via Inverse Transform of Confined Displacement Distribution. *J Phys Chem B* 119(45):14451-14459.
20. Bakshi S, Bratton BP, & Weisshaar JC (2011) Subdiffraction-limit study of Kaede diffusion and spatial distribution in live Escherichia coli. *Biophys J* 101(10):2535-2544.
21. Shindo H*, et al.* (1995) Solution structure of the DNA binding domain of a nucleoid-associated protein, H-NS, from Escherichia coli. *FEBS Lett* 360(2):125-131.
22. Lu XJ & Olson WK (2003) 3DNA: a software package for the analysis, rebuilding and visualization of three-dimensional nucleic acid structures. *Nucleic Acids Res* 31(17):5108-5121.
23. Abraham MJ*, et al.* (2015) GROMACS: High performance molecular simulations through multi-level parallelism from laptops to supercomputers. *SoftwareX* 1–2:19-25.
24. Li DW & Bruschweiler R (2010) NMR-based protein potentials. *Angew Chem Int Ed Engl* 49(38):6778-6780.
25. Desai SK*, et al.* (2016) The horizontally-acquired response regulator SsrB drives a Salmonella lifestyle switch by relieving biofilm silencing. *Elife* 5:5:e10747.
26. Spahn C, Endesfelder U, & Heilemann M (2014) Super-resolution imaging of Escherichia coli nucleoids reveals highly structured and asymmetric segregation during fast growth. *J Struct Biol* 185(3):243-249.